Ladder Capsule Network

Taewon Jeong [1] **Youngmin Lee** [1] **Heeyoung Kim** [1]

Abstract

We propose a new architecture of the capsule network called the ladder capsule network, which has an alternative building block to the dynamic routing algorithm in the capsule network (Sabour et al., 2017). Motivated by the need for using only important capsules during training for robust performance, we first introduce a new layer called the pruning layer, which removes irrelevant capsules. Based on the selected capsules, we construct higher-level capsule outputs. Subsequently, to capture the part-whole spatial relationships, we introduce another new layer called the ladder layer, the outputs of which are regressed lower-level capsule outputs from higher-level capsules. Unlike the capsule network adopting the routing-by-agreement, the ladder capsule network uses backpropagation from a loss function to reconstruct the lower-level capsule outputs from higher-level capsules; thus, the ladder layer implements the reverse directional inference of the agreement/disagreement mechanism of the capsule network. The experiments on MNIST demonstrate that the ladder capsule network learns an equivariant representation and improves the capability to extrapolate or generalize to pose variations.

1. Introduction

The convolutional neural network (CNN) has shown superhuman performances over the recent years for a wide range of computer vision tasks such as image classification, segmentation, detection, and tracking. In essence, a CNN predicts whether an object (e.g., face) exists by detecting the existence of features or object parts (e.g., eye, nose, mouth). However, CNN only captures the existence of features, and fails to capture the intrinsic spatial relationship between a part and a whole (e.g., the correct positions of the eye, nose, and mouth to form a face). This problem in CNN is due to the max-pooling that discards the information about the pose (position, size, orientation) of features, although it contributes to the extraction of translation-invariant features. As an alternative to the CNN, the capsule network (CapsNet), a new network architecture recently introduced by Sabour et al. (2017), learns an equivariant representation that is more robust to pose variations. CapsNet captures various pose information of the same feature by replacing scalar-output neurons in the CNN with vector-output capsules, and captures part-whole spatial relationships by replacing the max-pooling in the CNN with a dynamic routing algorithm. CapsNets have shown to outperform CNNs on digit recognition, even when using a dataset of highly overlapping digits (Sabour et al., 2017).

Although the dynamic routing algorithm has shown that it is effective in capturing part-whole relationships, it is inevitable that information on unnecessary lower-layer capsules would be included when constructing higher-layer capsules owing to the nature of the algorithm that expresses the higher-layer capsules by the weighted sum of many lower-layer capsules. Too many unnecessary capsules, similar to other over-parameterized deep learning networks, can cause confusion in delivering the necessary information to the upper layers and can ultimately lead to difficulties in performing the desired tasks (Costa et al., 2002).

In this paper, we propose a new architecture of capsule networks referred to as the ladder capsule network (L-CapsNet) based on an alternative building structure to the dynamic routing algorithm. We first demonstrate via experiments that not all lower-layer capsules are necessarily required to construct higher-layer capsules; only part of the capsules is sufficient to construct higher-layer capsules. To address this finding in the L-CapsNet, we introduce a new layer called the pruning layer, which is inspired by pruning methods that primarily aim at reducing the size of deep neural networks. The pruning layer removes the capsules with small activities and only uses the capsules with large activities. Subsequently, we can construct the higher-level capsules as a linear combination of the selected capsules from the pruning layer, similar to the CapsNet. Unlike the CapsNet that uses an iterative routing based on the agree-

[1] Department of Industrial and Systems Engineering, Korea Advanced Institute of Science and Technology (KAIST), Daejeon, Republic of Korea. Correspondence to: Heeyoung Kim <heeyoungkim@kaist.ac.kr>.

Proceedings of the 36^{th} International Conference on Machine Learning, Long Beach, California, PMLR 97, 2019. Copyright 2019 by the author(s).

ment between the predictions from lower-level capsules for constructing higher-level capsules and capturing the part-whole relationships, our model uses backpropagation from a loss function to reconstruct lower-level capsules from higher-level capsules. This reconstruction is performed in a new layer called the ladder layer. Similar to the ladder networks that proved their effective performance in semi-supervised learning (Rasmus et al., 2015), the ladder layer can effectively learn representative features for reconstruction using the feedback from lower-level capsules. Through these two building blocks—pruning and ladder layers, the L-CapsNet is shown to improve the capability to extrapolate or generalize to pose variations on the MNIST digits.

2. Background

2.1. Dynamic Routing of CapsNets

A capsule is a basic component of CapsNet, and it is defined as a group of neurons. The activity vector of a capsule represents the probability of existence of an entity (an object or an object part) by its length and the instantiation parameters of the entity by its orientation. Let $\{u_i \in R^d | i = 1, 2, ...N_l\}$ be the collection of the vector output of capsule i in layer l. To construct the vector output $v_j \in R^D$ of capsule j in layer $(l + 1)$, each u_i is first multiplied by the prediction matrix $W_{ij} \in R^{d \times D}$, producing the prediction vector $\hat{u}_{j|i} = W_{ij}u_i$; subsequently, a weighted sum of all prediction vectors, denoted by s_j, is computed as the total input of v_j as follows: $s_j = \sum_i c_{ij}\hat{u}_{j|i}$, where $\{0 \leq c_{ij} \leq 1\}$ are the coupling coefficients, which are determined through the dynamic routing algorithm summarized in Algorithm 1. Finally, v_j is calculated as $v_j = \frac{\|s_j\|^2}{1+\|s_j\|^2}\frac{s_j}{\|s_j\|}$ by applying the squashing function to s_j, which ensures that the length of the output vector represents the probability of existence of an entity.

Algorithm 1 Dynamic routing algorithm (Sabour et al., 2017)

```
Initialize logit parameters $b_{ij} = 0$ for all capsule $i$ in layer $l$ and capsule $j$ in layer $(l + 1)$.
for 1:$MaxIter$ do
    $c_{ij} = \frac{\exp(b_{ij})}{\sum_k \exp(b_{ik})}$ for all capsule $i$ in layer $l$.
    $s_j = \sum_i c_{ij}\hat{u}_{j|i}$ and $v_j = \frac{||s_j||^2}{1+||s_j||^2}\frac{s_j}{||s_j||}$ for all capsule $j$ in layer $(l + 1)$.
    $b_{ij} = b_{ij} + \langle \hat{u}_{j|i}, v_j \rangle$ for all capsule $i$ in layer $l$ and capsule $j$ in layer $(l + 1)$.
end for
```

In the dynamic routing algorithm, two points are to be emphasized. One is the linear relationship between the lower-level and higher-level capsules. The prediction vector $\hat{u}_{j|i}$ means the prediction of pose of entity j based on the pose of entity i. For example, if we know where someone's nose is, we can predict where his/her face is. Furthermore, if his/her nose is moved to some direction, the predicted position of his/her face is also moved to the same direction. Hence, it is reasonable to assume a linear relationship between the lower-level and higher-level capsules. This assumption is also used in the L-CapsNet to construct higher-level capsules based on lower-level capsules.

The other is the core idea of the dynamic routing algorithm. When we consider the pose of entity j, the core parts of entity j in the layer below should predict the pose of entity j consistently, but irrelevant parts are likely to predict the pose differently. Using the example above again, the nose and eyes are core parts of the face; therefore, the predictions of the face pose based on the poses of the nose and eyes should be similar: their predictions should agree. In contrast, the predictions of the face pose from the poses of a pencil or laptop (i.e., irrelevant parts) should disagree. Using this idea, the dynamic routing algorithm is expected to capture the part-whole relationship (lower-level and higher-level capsule relationship). In the algorithm, c_{ij} measures the importance of entity i in constructing entity j in the layer above. Moreover, a high value of c_{ij} indicates that the pose of entity j is similar with the predicted pose from entity i.

2.2. Pruning Techniques

Pruning is a method used to reduce network complexity by removing certain unimportant weights, neurons, or channels on the network (Luo et al., 2017). The primary purpose of pruning is to reduce the size of the network such that it can be used for devices with limited computing or storage capacity. For example, Molchanov et al. (2016) developed a greedy criteria-based pruning method that uses the Taylor expansion that approximates the parameter-importance evaluation. Aghasi et al. (2017) and Dong et al. (2017) proposed a layer-wise pruning method to reduce the complexity of deep neural networks. Structured pruning having various scale levels such as feature maps or kernels was used by Anwar et al. (2017) for the real-time application of a deep learning model. Pruning enabled the studies above to show similar or even better performance using a much smaller scale network than a larger network, as it could improve the generalization ability of deep learning models (Thodberg, 1991; Reed, 1993; Augasta & Kathirvalavakumar, 2013). The overfitting caused by a large number of parameters could be prevented by removing unnecessary connections in the networks.

For a similar objective, to improve the generalization of the capsule network, we use pruning as a layer that removes the information of unimportant capsules and retains only capsules that contain important information. This approach is similar to the stochastic activation pruning proposed for advanced defense (Dhillon et al., 2018), in that the pruning is based on the activity levels of neurons in the forward direction of the network. The operation of the pruning layer is similar to the k-max pooling (Kalchbrenner et al., 2014), which is a generalization of max pooling. However, one major difference exists: our pruning layer does not lose spatial information because the location information of the capsules is transferred to the upper layer by the so-called code vector. More detailed descriptions of the pruning layer and the code vector are presented in Section 3.1.

2.3. Ladder Networks

Over the recent years, many studies have demonstrated that supervised learning with auxiliary unsupervised representation learning can improve the network performance for supervised tasks (Suddarth & Kergosien, 1990). A ladder network, which adds an auxiliary task in the intermediate representation, is one example that is widely used in supervised (or semi-supervised) learning and showed remarkable performance on several tasks (Pezeshki et al., 2016; Dosovitskiy & Brox, 2016). Most ladder networks add auxiliary decoding layers, each of which corresponds to an encoding layer in the network for supervised learning, and each decoding layer targets at reconstructing the output of the corresponding encoding layer. Previous studies showed that this type of networks not only improves representation learning (Sønderby et al., 2016), but also achieves enhanced performance for supervised tasks (Zhang et al., 2016). The CapsNet (Sabour et al., 2017) also uses an additional reconstruction loss to encourage the digit capsules to encode the instantiation parameters of the input digit, which results in the improved performance of digit recognition, compared with the results from using only the margin loss.

Inspired by these, we adopt a ladder structure into the capsule network by introducing a new layer called the ladder layer, which forms an alternative building block to the dynamic routing algorithm. Unlike previous studies, our ladder directly links to supervised tasks and facilitates in capturing the part-whole relationship between capsules. This architecture is similar to the "what-where" autoencoder (Zhao et al., 2015), for which the "where" component is similar to the code vector that is introduced in the L-CapsNet. We discuss the ladder layer in more detail in Section 3.3.

3. Components of L-CapsNet

In this section, we describe the components of the L-CapsNet. The L-CapsNet consists of three components: pruning layer, weight construction and propagation layer, and ladder layer.

3.1. Pruning Layer

The use of pruning in the capsule network was motivated by a simple thought experiment. Let us use an example of a classification task between a human face and a car. The core entities of the face in the lower level could be the nose, eyes, or mouth, whereas the car's core entities could be wheels, roof, or mirror. If an input image corresponds to a human face, the routing algorithm is expected to predict the face pose based on the low-level capsules of the nose, eyes, and mouth. However, the predictions based on the wheel, roof, and mirror are also executed in the dynamic routing, even though their capsules are not activated. In fact, we only need to consider the results of the agreement/disagreement between the core entities of the face; predictions based on the car's capsules are not required.

This argument can be shown from our simple experiment to implement the CapsNet with the same architecture as in Sabour et al. (2017) on the MNIST dataset. After training the network, we found that the activities of some capsules were significantly higher than those of others. In addition, these highly activated capsules (u_i) tended to have relatively large coupling coefficients (c_{ij}) for the desired parent v_j. This indicates that the construction of higher-level capsules is primarily contributed by highly activated lower-level capsules; hence, the capsules with low activities need not be emphasized. Figure 1 illustrates the results with the digit "0". The graph shows the average length of u_i and the average value of c_{ij} of the 100 most active capsules over 5444 samples (total number of the digit "0" in the training set) on the left y-axis by the blue bar and the right-y axis by the red bar, respectively.

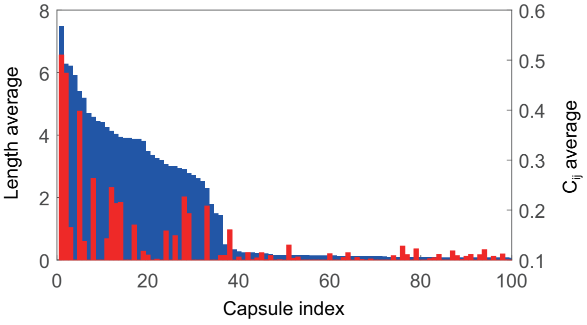

Figure 1: Length of u_i (left y-axis, blue bar) and value of c_{ij} (right y-axis, red bar) of the 100 most active lower-level capsules to predict the "0" digit capsule.

Inspired by these results, we introduce the pruning layer, which implements the selection of important lower-level capsules to ensure that only the outputs of the important capsules are sent to the layer above. We expect that the pruning layer not only reduces computational burden, but also improves the network generalization. The pruning layer collects the outputs of the K most active capsules. More specifically, consider the outputs of the level l capsules, $U^l = \{u_i \in B^d | i = 1, 2, ...n_l\}$, where B^d is the unit ball in R^d, and the corresponding activity level (or the probability of existence of an entity), $A^l = \{0 \leq a_i \leq 1 | i = 1, 2, ...n_l\}$. The orientation of u_i represents the pose of an entity, and the length of u_i represents the activity level, or the probability of existence of the entity, i.e., $a_i = \|u_i\|$. Before propagating the outputs in level l to level $(l+1)$, we select the K most active capsules. Let $a_{(i)}$ denote the ith highest activity level in A^l such that $a_{(1)} > a_{(2)} > ... > a_{(n)}$. Further, let $I_{(m)}$ denote the ordering index for the mth lowest activity level within $\{i | a_i \geq a_{(K)}\}$. Subsequently, we can collect the outputs of the K most active capsules as $\{u_{I_{(m)}} \in R^d | m = 1, 2, ...K\}$. Based on this collection, we can construct $U^l_K \in R^{K \times d}$ matrix, where the pth row is equal to $u_{I_{(p)}}$. We also consider one-hot encoded vectors $c^l \in (0,1)^{n_l}$ from the index set $\{i | a_i \geq a_{(K)}\}$, which we call the code vector. The code vector restores the information about which capsules are selected, and it contains the information about which capsules in U^l are used to form U^l_K. For level $(l+1)$, we only propagate U^l_K and c^l, instead of the whole capsule output U^l; subsequently, we construct higher-level capsules in level $(l+1)$. Figure 2 illustrates an example of the pruning layer with $n_l = 6$ and $K = 3$: when the three capsules u_1, u_4, and u_6 are selected among u_i, $i = 1, \ldots, 6$, the code vector becomes $c^l = (1, 0, 0, 1, 0, 1)$.

3.2. Weight Construction and Propagation Layer

We propagate each row of U^l_K to higher-level capsules by applying a linear operator, as discussed in Section 2.1. Recall that the CapsNet sets the prediction matrix W_{ij} as a linear operator between all lower-level and higher-level capsules. That is, predictions $\hat{u}_{j|i}$ from all lower-level capsules by multiplying W_{ij} are propagated to the layer above to construct higher-level capsule outputs. In contrast, the L-CapsNet propagates only part of the capsules selected in the pruning layer, U^l_K, to the next level above; thus, the same operation with W_{ij} cannot be directly used. Instead of W_{ij}, we use the code vector c^l, which contains the information about which capsules are highly active. We define a function of the code vector $\{f_{j|i}(c^l) \in R^{d \times D}\}$, which is a linear operator for propagating the ith row in U^l_K to the capsule j in layer $(l+1)$.

Moreover, we define another non-negative function of the code vector $p_j(c^l) = (p_{j|1}(c^l), p_{j|2}(c^l), \ldots, p_{j|K}(c^l))$, which determines how much contribution comes from different output vectors of the layer below. Let u^l_i denote the ith row of U^l_K and $\tilde{u}_{j|i}$ denote the prediction made by a capsule i. We have $\tilde{u}_{j|i} = u^l_i f_{j|i} \in R^D$. Subsequently, we compute a *partial* input of capsule j in layer $(l+1)$, denoted by s^{l+1}_j, as follows:

$$s^{l+1}_j = \sum_{i=1}^{K} p_{j|i}(c^l) \tilde{u}_{j|i} \in R^D. \tag{1}$$

We used the word "partial," because other components (that will be discussed in Section 3.3) are also used to construct the output of capsule j in layer $l+1$, v^{l+1}_j. More precisely, s^{l+1}_j only represents the pose of entity j in layer $l+1$. In the layer above, we obtain the activity level and by multiplying it by $\frac{s^{l+1}_j}{\|s_j\|}$, we compute the total output of v^{l+1}_j. In the L-CapsNet, the functions of the code vector, $f_{j|i}$ and p_j, are architecture from a deep convolutional neural network; we train all parameters of the network via backpropagation. This is different from the dynamic routing algorithm: we train the contribution rate of propagation, $p_j(c^l)$, while the dynamic routing determines c_{ij} using an iterative routing algorithm.

3.3. Ladder Layer

The ladder layer is designed to capture the part-whole relationship; it plays a similar role as the dynamic routing algorithm, but is based on a different idea. Recall that in the dynamic routing algorithm, predictions made from lower-level capsules are investigated if they agree. The L-CapsNet focuses on the reverse directional inference; lower-level capsules are regressed from higher-level capsules. The primary idea of the ladder layer is that if higher-level capsules are well constructed, we can subsequently infer the pose of the core entities in the layer below. Using the simple example of Section 2.1, if we know the face pose such as the location and orientation, subsequently we can well infer the pose of the core entities of the face, nose, and eyes; however, it is difficult to infer the pose of irrelevant entities such as a pencil or laptop. Recall that U^l_K is constructed by selecting the K most active capsules, which correspond to the entities with high probability of existence. If the elements of U^l_K are indeed the core entities of capsule j in layer $l+1$, then we can expect that regression from s^{l+1}_j to U^l_K performs well.

As the lower-level and higher-level capsules are linked by a linear relationship, the regression from s^{l+1}_j to U^l_K is also assumed to be linear. We introduce a linear regression operator $f^{reg}_j(c^l) \in R^{K \times d \times D}$, which is another function of the code vector used for the regression of U^l_K from v^{l+1}_j. The regressed U^l_K from v^{l+1}_j is denoted by $\hat{u}^{reg}_j$:

$$\hat{u}^{reg}_j = f^{reg}_j(c^l)(s^{l+1}_j)^T \in R^{K \times d}. \tag{2}$$

As u^l_j lies on the unit ball B^d, we apply the squashing function to $\hat{u}^{reg}_j$ for down scaling, resulting in u^{reg}_j in Eq.(3). Although the squashing function is nonlinear, it preserves

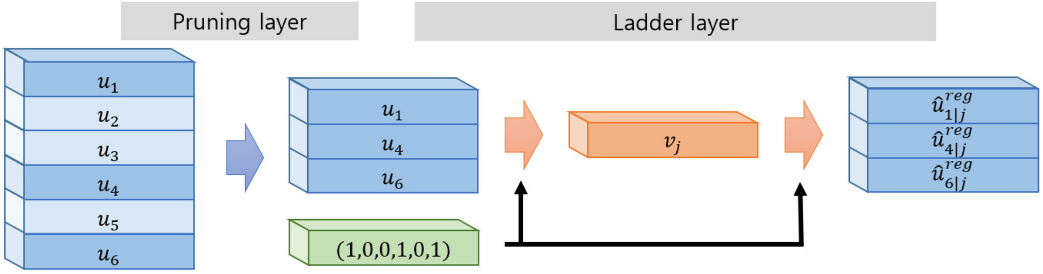

Figure 2: Illustration of the pruning and ladder layers

the input orientation; therefore, the regression of the pose is still valid after applying the squashing function.

$$u_j^{reg} = \frac{\|\hat{u}_j^{reg}\|^2}{1+\|\hat{u}_j^{reg}\|^2}\frac{\hat{u}_j^{reg}}{\|\hat{u}_j^{reg}\|} \in B^{K\times d}. \tag{3}$$

Subsequently, we define an L2-norm-based similarity measure, denoted by d_j, between u_j^{reg} and U_K^l. The measure d_j allows us to numerically evaluate the part-whole relationship between lower-level and higher-level capsules:

$$d_j = \exp(-\gamma\|u_j^{reg} - U_K^l\|^2), \tag{4}$$

where $\|u_j^{reg} - U_K^l\|^2 = \frac{1}{K}\sum_{i=1}^{K}\|u_{i|j}^{reg} - u_i^l\|^2$, where $u_{i|j}^{reg}$ denotes the ith row of u_j^{reg}, and γ is a non-negative hyperparameter. A value of d_j close to one indicates a good fit of the regression model, resulting in lower-level entities appropriately posed for constructing higher-level entities. Hinton et al. (2018) indicated the importance of sensitiveness to the difference between good and very good agreement, which is one of deficiencies of the dynamic routing algorithm. Hence, we choose the hyperparameter $\gamma = 5.12$, which solves for $\exp(-0.01\gamma) = 0.95$ to ensure a good fit of the regression model for a well-suited relationship between lower-level and higher-level entities. We let d_j represent the activity of the capsule j in layer $(l+1)$. Using d_j, the total output of capsule j in layer $l+1$ is given by $v_j^{l+1} = d_j\frac{s_j^{l+1}}{\|s_j^{l+1}\|}$.

Recall that c^l provides the information about which entity's pose is represented in each row of U_K^l. Therefore, c^l informs f_j^{reg} about the entities that should be regressed from s_j^{l+1}, which makes the ith row of $\hat{u}_j^{reg}$ reconstruct u_i^l. It is noteworthy that the ladder layer trains all weights via backpropagation, unlike the CapsNet that uses an iterative routing. This reduces the computational cost of the L-CapsNet. A comparison of computation time between the CapsNet and L-CapsNet is presented in Section 5.2.

4. Loss on L-CapsNet

Sabour et al. (2017) proposed the margin loss for classification using the capsule network. We also applied this loss, which is expressed on the L-CapsNet as follows:

$$\begin{aligned} L_k^{margin} &= T_k \max(0, m^+ - d_k)^2 \\ &\quad +\lambda(1-T_k)\max(0, d_k - m^-)^2, \end{aligned}$$

where T_k's are outputs of the one-hot encoded labels; m^+, m^-, and λ are non-negative hyperparameters; d_i is the activity level of capsule i in the final layer; further, the number of capsules in the final layer should be the same as the number of labels. In Section 5, we trained the L-CapsNet with the margin loss with $m^+ = 0.9$, $m^- = 0.1$, and $\lambda = 0.5$. In addition, we found that adding the loss of difference between the code vector and lower-level activity level, $\|c^l - A^l\|^2$, would be helpful for training; thus we trained the L-CapsNet with the loss

$$L = L^{margin} + \epsilon\|c^l - A^l\|^2$$

with $\epsilon = 0.0001$. We used the Adam optimizer with exponentially decaying learning rate starting from 0.001.

5. L-CapsNet Architecture and Experiments

5.1. L-CapsNet Architecture

The general architecture of the L-CapsNet is depicted in Figure.3. We start with a convolutional layer having a 9×9 kernel and 256 channels with a stride of 1 and the ReLu activation function. This layer propagates the activities of the local feature detectors to the primary capsule layer, similar to the work of Sabour et al. (2017), by applying 8 convolution units with a 9×9 kernel, 32 channels, and a stride of 2. Subsequently, for an $I\times I$ pixel image, the primary capsules have a total of $n_I \times n_I \times 32$ 8D capsule outputs, where $n_I = \text{ceil}(\frac{I-16}{2})$. Each primary capsule output sees the output of all convolution units whose receptive fields overlap with the location of the center of the capsule. We first construct $n_l = n_I \times n_I \times 32$ primary capsule inputs $t_i \in R^8$; subsequently, we obtain the primary capsule output $u_i = \text{squash}(t_i)$, by applying the squash function, and the corresponding activity $a_i = \frac{\|t_i\|^2}{1+\|t_i\|^2}$. Subsequently, the primary capsule outputs are propagated to the pruning layer, which selects the K most active capsules, forming U_K^{pri},

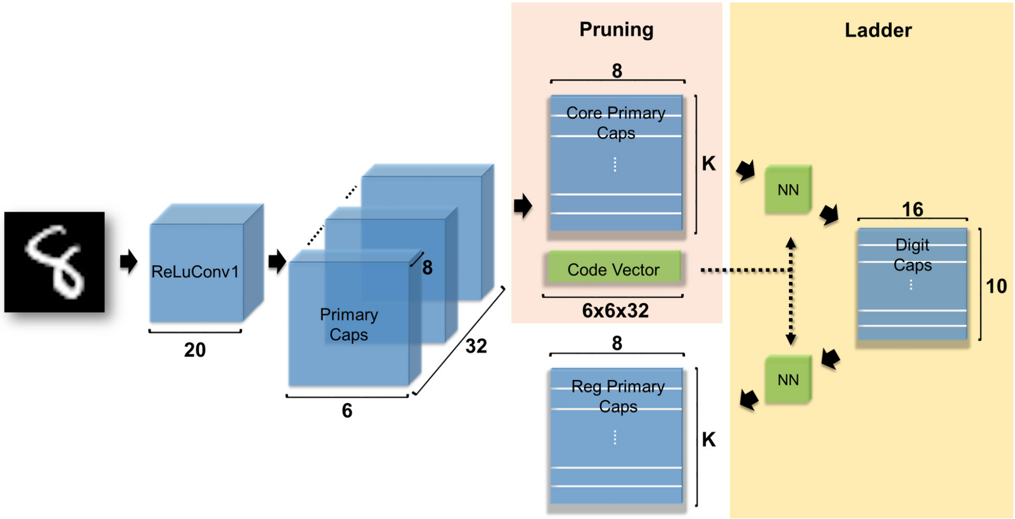

Figure 3: L-CapsNet architecture

Table 1: Architecture of the function of the code vector

	$f_{j\|i}(c^{pri})$	$f_j^{reg}(c^{pri})$	$p_j(c^{pri})$
1st layer	fully connected, activation: Relu		
output dim	$8 \times 16 \times 3$	$8 \times 16 \times 3$	$K \times 3$
2nd layer	fully connected, activation: Relu		
output dim	$8 \times 16 \times 2$	$8 \times 16 \times 2$	$K \times 2$
3rd layer	fully connected, activation: Relu		
output dim	8×16	8×16	K
4th layer	fully connected, activation: linear ($f_{j\|i}(c^{pri})$, $f_j^{reg}(c^{pri})$), sigmoid($p_j(c^{pri})$)		
output dim	$8 \times 16 \times K$	$8 \times 16 \times K$	K

which we call the core primary capsules, and then the corresponding code vector c^{pri} is obtained. Based on c^{pri}, we construct $f_{j|i}(c^{pri})$, $p_j(c^{pri})$, and $f_j^{reg}(c^{pri})$ using a combination of fully connected layers and convolution layers. More detailed structures are presented in Table 1. By applying those linear operators for propagation (i.e., $f_{j|i}(c^{pri})$ and $p_j(c^{pri})$) and for regression (i.e., $f_j^{reg}(c^{pri})$), we obtain the digit capsules and regressed primary capsules. As mentioned in Section 4, the number of digit capsules equals the number of labels, and we set the dimension of the digit capsules to 16. By computing the similarity between the core primary capsules and the regressed primary capsules using Eq.(4), the activity of each digit capsule is obtained, which is subsequently used to compute the loss in Section 4.

5.2. Experiments on MNIST

To evaluate the performance of the L-CapsNet, we performed two experiments. For the first experiment, we trained 60,000 images and tested 10,000 images of the 28×28 MNIST. For the second experiment, we trained 60,000 images of the 40×40 expanded MNIST, and tested 10,000 images of the affNIST. We assumed the same experimental environment (i.e., 9×9 kernel on ReLuConv1 and PrimaryCaps) as in Sabour et al. (2017) on both experiments. This setting produces 1152 capsules for the MNIST experiment and 4608 capsules for the expanded MNIST and affNIST experiment. Furthermore, to consider various ratios of the number of selected capsules to the total capsules, we assumed more experimental settings with the kernel size 15×15. In the MNIST experiment, we change the kernel size on PrimaryCaps from 9×9 to 15×15, and in the expanded MNIST and affNIST experiment, we set the kernel size 15×15 on both layers. These settings produce 288 and 1152 primary capsules on MNIST and affNIST, respectively. We performed the experiments with several values of K for pruning. Table 2 shows the test error for each case, together with the results of the CNN and CapsNet reported in Sabour et al. (2017).

Although the L-CapsNet resulted in higher test errors on MNIST classification, it dramatically outperformed on the affNIST test set. Recall that the expanded MNIST is con-

Table 2: Test error results of L-CapsNets

Method	K	MNIST(%)	affNIST(%)
CNN (Sabour et al., 2017)	-	0.39	34.0
CapsNet (Sabour et al., 2017)	-	0.25	21.0
L-CapsNet (9 × 9 kernel)	50	0.74	13.0
L-CapsNet (9 × 9 kernel)	70	0.50	12.5
L-CapsNet (9 × 9 kernel)	100	0.80	13.2
L-CapsNet (15 × 15 kernel)	50	0.69	12.5
L-CapsNet (15 × 15 kernel)	70	0.73	12.2
L-CapsNet (15 × 15 kernel)	100	0.79	13.1

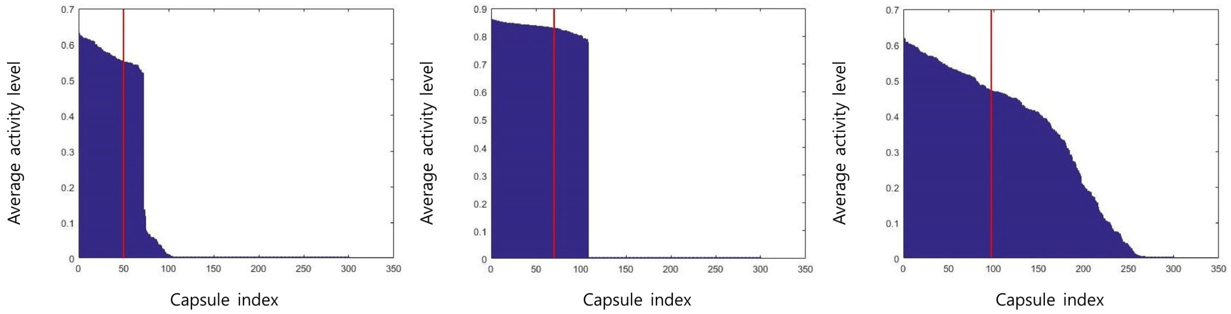

(a) K=50 (b) K=70 (c) K=100

Figure 4: Activity levels of the primary capsules on L-CapsNet

structed by translating MNIST, whereas affNIST is constructed by MNIST's affine transformation, i.e., affNIST incorporates more variations (e.g., rotation). The outperforming results on affNIST show that the L-CapsNet learns an equivariant representation that is more robust to pose variations on MNIST digits than the CapsNet.

Moreover, we compare the computation time of the L-CapsNet and CapsNet. We varied the value of K in the L-CapsNet as 50, 70, and 100, while varying the number of routing iterations (denoted by r) in the dynamic routing algorithm in the CapsNet as 3, 4, and 5. Table 3 presents the average computation time of 1 training iteration over 100 batch samples on MNIST, with standard errors in parentheses. The results show that the L-CapsNet significantly reduces the computation time. This may be because only the selected lower-level capsules from the pruning layer are sent to the layer above, and all weights are trained via backpropagation through the ladder layer in the L-CapsNet, while all lower-level capsules are used in the dynamic routing algorithm with several routing iterations in the CapsNet.

Table 3: The average computation time of 1 training iteration over 100 batch samples on MNIST. r: the number of routing iterations. Standard errors in parentheses.

Method	Computation time, in seconds
L-CapsNet ($K = 50$)	0.2034 (0.010)
L-CapsNet ($K = 70$)	0.2159 (0.008)
L-CapsNet ($K = 100$)	0.2953 (0.001)
CapsNet ($r = 3$)	1.732 (0.026)
CapsNet ($r = 4$)	2.123 (0.041)
CapsNet ($r = 5$)	2.656 (0.085)

5.3. Analysis of the Effects of K

In the L-CapsNet, only K most active capsules are used for classification tasks. Recall the example in Section 3.1 again, when the input is a human face, we hope that the core entities (e.g., nose, eyes, and mouth) are captured in K most activate capsules, while capsules for representing irrelevant entities (e.g., wheels and mirrors) are deactivated. In other words, we hope that the L-CapNet clearly discriminates capsules for core entities versus irrelevant entities. We found from our experiments that this could be achieved by appropriately selecting the number of K.

We performed an analysis to see the effects of the hyperparameter K in the L-CapsNet. Figure 4 illustrates the average activity levels of 300 most active primary capsules on the L-CapsNet over 5444 samples of digit "0" in the

MNIST training set for K values of 50, 70, and 100. We can see that for low K values (i.e., K=50, 70), the activity levels are extremely high or low. That is, the active and inactive capsules are distinguished clearly. This supports our adoption of K motivated by the need for using only important capsules for robust performance. When $K = 100$, the distinction between active and inactive capsules is not as clear as the cases of K=50 and 70, maybe because it is not very effective in capturing disentangled entities and their poses using more capsules than actually needed. In contrast, when K is low, each capsule may capture a disentangled entity and its pose, which results in clear discrimination between active and inactive capsules, which represent core and irrelevant entities, respectively. As Lenssen et al. (2018) pointed out the importance of disentangled representation for equivariance, for our experiments, low K values would be preferred.

6. Conclusion

In this paper, we proposed a new building block of the capsule network that removes irrelevant capsules without losing information about the spatial relationship between lower-level and higher-level entities, based on our fining that only part of the entities (i.e., core entities) significantly contributes to capturing the part-whole spatial relationships. While the CapsNet captures the part-whole relationships by using an iterative routing-by-agreement, the L-CapsNet achieves the same goal by using both the pruning and ladder layers. More specifically, the pruning layer selects relevant lower-level capsules based on the activity level, using the fact that the activity level represents the probability of existence of an entity. In fact, we showed that highly active lower-level capsules tend to have large coupling coefficients for the desired parent (Figure 1) and that the L-CapsNet clearly discriminates relevant and irrelevant capsules using the activity level (Figure 4). Subsequently, the higher-level capsules can be constructed as a linear combination of the selected lower-level capsules. Unlike the CapsNet that takes the inner product between higher-level capsule and the prediction from the layer below as the "agreement" rule, the L-CapsNet takes how well lower-level capsule outputs are regressed from higher-level capsules as the agreement rule.

We select the K most active capsules through the pruning layer, and subsequently propagate the activities of only the selected capsules into the layer above, from which we can expect the robust capability on the network. However, the method to determine the appropriate K value according to the characteristics of data or tasks should be further studied. In our MNIST & affine MNIST experiments, the value of K selected at a rate of approximately 6% of the total capsules produced the best results. Another important component of the L-CapsNet is the ladder layer. It is motivated by the reverse directional inference of the agreement/disagreement rule for the CapsNet. Based on our outperforming results on the affNIST data, we may conclude that the ladder layer provides the extrapolation capability or robustness on the L-CapsNet.

The reverse directional inference was similarly considered in Hinton et al. (2018). In their work, Hinton et al. (2018) approximate the mispredictions by higher-level capsules of lower-level capsule outputs by using the negative log probability density, avoiding the expensive matrix inversion of the prediction matrix W_{ij}. The L-CapsNet learns the inverse linear transformation f^{reg} with a neural network rather than exactly inverting W_{ij} or $f_{j|i}$.

For more extensive research, we plan to develop an algorithm for a bi-directional agreement/disagreement mechanism, based on the idea that we can predict not only higher-level capsule outputs from lower-level capsules, but can also regress lower-level capsule outputs from higher-level capsules. We expect this exchangeability to enable more robust capsule outputs to be extracted and improve the task performance. The code for L-CapsNet is available at `https://github.com/taewonjeong/L-CapsNet`.

Acknowledgements

The authors thank the reviewers for reviewing the paper and providing valuable comments. This work was supported by the National Research Foundation of Korea (NRF) grant funded by the Korea government (MSIT) (No.2018R1C1B6004511).

References

Aghasi, A., Abdi, A., Nguyen, N., and Romberg, J. Net-trim: Convex pruning of deep neural networks with performance guarantee. In *Advances in Neural Information Processing Systems*, pp. 3177–3186, 2017.

Anwar, S., Hwang, K., and Sung, W. Structured pruning of deep convolutional neural networks. *ACM Journal on Emerging Technologies in Computing Systems (JETC)*, 13(3):32, 2017.

Augasta, M. G. and Kathirvalavakumar, T. Pruning algorithms of neural networksa comparative study. *Central European Journal of Computer Science*, 3(3):105–115, 2013.

Costa, M. A., Braga, A. P., and de Menezes, B. R. Improving neural networks generalization with new constructive and pruning methods. *Journal of Intelligent & Fuzzy Systems*, 13(2-4):75–83, 2002.

Dhillon, G. S., Azizzadenesheli, K., Lipton, Z. C., Bernstein, J., Kossaifi, J., Khanna, A., and Anandkumar, A.

Stochastic activation pruning for robust adversarial defense. *arXiv preprint arXiv:1803.01442*, 2018.

Dong, X., Chen, S., and Pan, S. Learning to prune deep neural networks via layer-wise optimal brain surgeon. In *Advances in Neural Information Processing Systems*, pp. 4860–4874, 2017.

Dosovitskiy, A. and Brox, T. Inverting visual representations with convolutional networks. In *Proceedings of the IEEE Conference on Computer Vision and Pattern Recognition*, pp. 4829–4837, 2016.

Hinton, G. E., Frosst, N., and Sabour, S. Matrix capsules with EM routing. In *International Conference on Learning Representations*, 2018.

Kalchbrenner, N., Grefenstette, E., and Blunsom, P. A convolutional neural network for modelling sentences. In *Proceedings of the 52nd Annual Meeting of the Association for Computational Linguistics (Volume 1: Long Papers)*, volume 1, pp. 655–665, 2014.

Lenssen, J. E., Fey, M., and Libuschewski, P. Group equivariant capsule networks. *arXiv preprint arXiv:1806.05086*, 2018.

Luo, J.-H., Wu, J., and Lin, W. Thinet: A filter level pruning method for deep neural network compression. In *Proceedings of the IEEE Conference on Computer Vision and Pattern Recognition*, pp. 5058–5066, 2017.

Molchanov, P., Tyree, S., Karras, T., Aila, T., and Kautz, J. Pruning convolutional neural networks for resource efficient inference. *Proceedings of the International Conference on Learning Representations*, 2016.

Pezeshki, M., Fan, L., Brakel, P., Courville, A., and Bengio, Y. Deconstructing the ladder network architecture. In *International Conference on Machine Learning*, pp. 2368–2376, 2016.

Rasmus, A., Berglund, M., Honkala, M., Valpola, H., and Raiko, T. Semi-supervised learning with ladder networks. In *Advances in Neural Information Processing Systems*, pp. 3546–3554, 2015.

Reed, R. Pruning algorithms-a survey. *IEEE transactions on Neural Networks*, 4(5):740–747, 1993.

Sabour, S., Frosst, N., and Hinton, G. E. Dynamic routing between capsules. In *Advances in Neural Information Processing Systems*, pp. 3859–3869, 2017.

Sønderby, C. K., Raiko, T., Maaløe, L., Sønderby, S. K., and Winther, O. Ladder variational autoencoders. In *Advances in neural information processing systems*, pp. 3738–3746, 2016.

Suddarth, S. C. and Kergosien, Y. Rule-injection hints as a means of improving network performance and learning time. In *Neural Networks*, pp. 120–129. Springer, 1990.

Thodberg, H. H. Improving generalization of neural networks through pruning. *International Journal of Neural Systems*, 1(04):317–326, 1991.

Zhang, Y., Lee, K., and Lee, H. Augmenting supervised neural networks with unsupervised objectives for large-scale image classification. In *International Conference on Machine Learning*, pp. 612–621, 2016.

Zhao, H., Wang, Z., Wu, H., Xiao, Q., Yao, W., Wang, E., Liu, Y., and Wei, M. Stat3 genetic variant, alone and in combination with stat5b polymorphism, contributes to breast cancer risk and clinical outcomes. *Medical Oncology*, 32(1):375, 2015.